Solar Energy Materials & Solar Cells 113 (2013) 1–6

Contents lists available at SciVerse ScienceDirect

Solar Energy Materials & Solar Cells

journal homepage: www.elsevier.com/locate/solmat

Improvement of performance of GaAs solar cells by inserting self-organized InAs/InGaAs quantum dot superlattices

A. Sayari [a,*], M. Ezzidini [b], B. Azeza [b], S. Rekaya [b], E. Shalaan [c], S.J. Yaghmour [a], A.A. Al-Ghamdi [c], L. Sfaxi [d], R. M'ghaieth [b], H. Maaref [b]

[a] Department of Physics, Faculty of Science, King Abdulaziz University, North Jeddah Branch, P.O. Box 80203, Jeddah 21589, Kingdom of Saudi Arabia
[b] Laboratoire de Micro-Optoélectroniques et des Nanostructures, Université de Monastir, Tunisia
[c] Department of Physics, Faculty of Science, King Abdulaziz University, P.O. Box 80203, Jeddah 21589, Kingdom of Saudi Arabia
[d] Laboratoire de Micro-Optoélectroniques et des Nanostructures, Université de Sousse, Tunisia

ARTICLE INFO

Article history:
Received 19 December 2012
Accepted 22 January 2013
Available online 21 February 2013

Keywords:
Quantum dot solar cells
III–V Heterostructures
Multi-stacking
Spectroscopic ellipsometry.

ABSTRACT

This study demonstrates the feasibility of improving the performance of a quantum dot (QD) intermediate band solar cell (SC) by capping an InGaAs layer on the InAs QDs and inserting GaAs spacer layers. For comparison, a GaAs reference SC of the same p-i-n structure but without InAs QDs is grown. The two devices were grown by solid source molecular beam epitaxy (SS-MBE) on epiready (001) n^+-GaAs substrates and the InAs QDs structure is highly stacked and well-aligned. The two SCs were investigated by sepectroscopic ellipsometry (SE), in the photon energy range of 1–6 eV, photoluminescence (PL) and photo-absorption measurements. The two major spectral features observed in the dielectric function spectra of the InAs QDs SC at ~3 eV and ~4.5 eV are attributed to the E_1 and E_2 critical point structures of GaAs and InAs, respectively. The PL spectrum of the InAs QDs in the GaAs matrix is higher and presents an asymmetric shape, which indicated the growth of a high-quality multistacked InAs QDs structure and the contribution of larger and relatively smaller QDs to PL spectrum. The electrical conversion at the infrared range of λ=850–1300 nm for the InAs QDs SC is demonstrated by photocurrent spectra. The enhanced absorption performance (up to 1280 nm) of the QDs SC was attributed to the optical absorption from InAs QDs, wetting layer and InGaAs layer of the InAs/InGaAs/GaAs QD heterostructure.

1. Introduction

Considerable improvements in Si and III–V semiconductor solar cell (SC) performance have been made in the last decade [1–3]. For example, a 23% Si cell [4] and a 24.8% GaAs cell [5] under one sun condition have been achieved. However, the authors were used antireflection coating to obtain such efficiency because surface of these SC materials reflect back a significant portion of the incident sunlight (~30%) [6,7].

Recently, self-organized InAs quantum dots (QDs) have attracted much attention as medium for SCs because their incorporation in the middle layer enhances the photocurrent of the SC [8–11]. The quantized energy states of stacked QDs could function as an intermediate band for efficient absorption of photon in the SC structure [12,13]. In order to realize high performance photovoltaic devices, it is important to grow QD superlattices (SLs) that have periodically and uniformly distributed QDs by using a multiple stacking technique since the electronic properties of QDs depend on their size, shape and surrounding matrix [14,15]. It is possible to tailor the absorption spectrum of the InAs QD by the growth rate, temperature and in situ annealing treatment to enhance its absorption with respect to the solar spectrum [16,17]. However, the crystal quality of InAs QDs degrades as the number of QD layers increases due to the internal strain which causes dislocations that thread up from the QD layers to the device surface. As a consequence, the performance of InAs/GaAs QD SCs also degrades as the number of QD layers increases [18]. Authors suggested a strain compensation growth technique by inserting buffer layers in the InAs/GaAs heterostructure to overcome this problem [19]. For enhancement of absorption, vertical stacks of InAs QDs embedded in InGaAs/GaAs are preferred, but In segregation has to be considered, especially when an in situ annealing treatment is done [20].

Among the various methods used to qualify the optical properties of films, spectroscopic ellipsometry (SE) measurement is a very sensitive tool [21,22]. It allows the straightforward measurement of optical constants from the two independent ellipsometry parameters (ψ, Δ) [21]. Particularly, the real and imaginary parts

* Corresponding author. Tel.: +966 2 695 2287; fax: +966 2 695 2278.
E-mail address: amor.sayari@laposte.net (A. Sayari).

0927-0248/$ - see front matter © 2013 Elsevier B.V. All rights reserved.
http://dx.doi.org/10.1016/j.solmat.2013.01.033

of the dielectric function are determined in a straightforward manner and approximations in a subsequent Kramers–Kronig analysis are avoided. Therefore, if the SE results of a unit layer are analyzed, the performance of the SC composed of epitaxial layers could be predicted, and optimization of the SC might be easier and faster [23,24]. However, few studies have been reported on SE for extracting optical constants of QD SCs.

In this study, we report on the characteristics of two GaAs-based SCs, the first contains stacking of well-aligned 5-layer InAs QDs grown using the intermittent deposition of $In_{0.13}Ga_{0.87}As$ and the second is a reference GaAs SC used for comparison. The 5-layer InAs QDs were grown without any degradation in crystal quality and $In_{0.13}Ga_{0.87}As$ was used as strain compensated layer. The techniques used for characterization of the two devices are SE, photoluminescence (PL) and photo-absorption. The photo-absorption spectrum of the InAs QDs SC was extended toward a wavelength (~1280 nm) longer than the GaAs band gap (880 nm). The enhanced absorption performance of the InAs QDs SC was attributed to the optical absorption from InAs QDs, wetting layer and InGaAs layer.

2. Experimental details

Fig. 1(a) and (b) illustrates a schematic diagram of the two SC structures with and without InAs QDs SL. The epitaxial layers were grown on epiready n^+-GaAs (001) substrate using solid-source molecular beam epitaxy (SS-MBE) with Riber MBE 32 P system. Following oxide desorption at 600 °C under As_4 ambient condition, in-situ reflection high energy electron diffraction (RHEED) was used to observe the surface reconstruction. When a clear (2×4) reconstruction appeared, we decrease the temperature to 520 °C to start growth of a 250 nm n^+-doped GaAs buffer with a doping density of 2×10^{18} cm^{-3} followed by a 1000 nm n-doped GaAs base layer with a doping density of 1×10^{17} cm^{-3}.

The substrate temperature is then lowered and stabilized to 500 °C for the deposition of the active region. This later consists of 5 stacks InAs/$In_{0.13}Ga_{0.87}As$/GaAs QD heterostructure sandwiched by 80 nm intrinsic GaAs layer. For the InAs QDs growth, we deposited nominally 2.5 monolayer (ML) with a rate of 0.12 ML/s. Since the InAs QDs were formed in the Stranski–Krastanov growth mode, this has led to a wetting layer of about 1.7 ML thickness and the QDs on top of it. The brag spots in diagram RHEED, Fig. 1(c), confirm the three dimensional growth mode observed after InAs QDs deposition. After, a 5 nm $In_{0.13}Ga_{0.87}As$ strain compensated layer and 33 nm GaAs spacer were deposited. The diagram (d) inserted in Fig. 1 shows a highly two dimensional growth mode observed during the growth of InGaAs strain compensated layer. At the end, a 500 nm p-doped GaAs emitter layer (2×10^{17} cm^{-3}) followed by a 100 nm GaAs p^+-doped contact layer (5×10^{18} cm^{-3}) were grown on top of the structure. Silicon (Si) and Beryllium (Be) were used as n- and p-type dopants. During the growth, the temperature was calibrated by a pyrometer. The growth rate was measured by RHEED specular spot oscillations. A GaAs reference SC of the same p-i-n structure but without InAs QDs was grown, with a 350 nm-thick i-layer.

SE measurements were performed using a J. A. Woollam Variable Angle Spectroscopic Ellipsometer (VASE) M-2000 model which has photon energy range of 1–6 eV. This equipment includes well-made software to fit experimental data and modeled parameters. Ellipsometric spectra (ψ, Δ) were measured to derive optical parameters by using adequate model and multilayer model of roughness heterostructures. The SE measurements were carried out at room temperature in the 1–6 eV photon energy region, with angle of incidence $\phi=70^\circ$.

The PL and the spectral response (SR) measurements were performed to examine the optical transitions of the QD SCs. The PL measurements are performed using the 514.5 nm line of a continuous wave argon laser as the excitation source and a nitrogen cooled InGaAs detector coupled to a monochromator for the detection. For the photocurrent measurement, Indium Zinc (InZn) alloys was used for the top ohmic contact and indium (In) for the bottom contact of the SC, without antireflection layer. The SR measurement was performed at 300 K using a photocurrent spectroscopy bench comprising a 100 W tungsten halogen lamp, CVI CM110 1/8 monochromator and a kiethley 6485 picoammeter.

3. Results and discussions

Ellipsometry measurements were performed to determine the optical constants of the different layers in the GaAs and the InAs/InGaAs QD SCs. The model fit to the experimental data for the two devices is shown in Fig. 2. As can be seen the fit shows excellent agreement with the measured data in the 1–6 eV energy range. It can be seen in Fig. 3 that the ψ peaks in Fig. 2 correspond to excitonic absorption peaks at ~3 and 5 eV. This is associated with a rapid change of the refractive index from 2.5 to 3.5 eV and from 4 to 5 eV. At the low photon energy, the SE spectra show weak oscillations which are due to multiple reflections within the film interfaces.

The effective refraction index, n, and the extinction coefficient, k, of the InAs/InGaAs QDs SC are extracted from the ellipsometric parameters by utilizing a multilayer model, and are shown in Fig. 3. It is observed that changes in optical absorption are primarily influenced by the InAs/InGaAs QD layers while the refractive index of the SC is determined by the GaAs layers. The contribution of each layer is then accumulated to produce an optical interference that results in the exciton absorption peak and the rapid change of the index of refraction near the excitonic lines.

Fig. 4 shows the measured (a) real and (b) imaginary parts of the dielectric function of InAs QDs SC at 300 K for the energy range from 1 to 6 eV. The real and imaginary parts follow different patterns. The variation of the dielectric function with photon energy indicates that some interactions between photons and electrons in the films are produced in the energy range 1–6 eV. The two major spectral features are the E_1 and E_2 critical point (CP) structures at ~3 eV and ~4.5 eV, respectively [25,26]. To quantitatively determine the energy position of the different interband transitions, we took the zero crossing of the second derivative spectrum of the imaginary part of the pseudodielectric function. The different transition energies obtained are summarized in Table 1. Fig. 5 shows the second energy derivative spectrum of the imaginary part of the pseudodielectric function shown in Fig. 4. The two peaks at 2.9 and 3.1 eV correspond, respectively, to the E_1 and $E_1+\Delta_1$, interband transitions in GaAs. However, the two closely positioned peaks at about 4.4 eV and 4.7 eV, are caused by the CP transitions E_0' and E_2, respectively, in InAs QD layers [26]. We note that the contribution of the $E_1+\Delta_1$ CP energy (2.74 eV) [26] of InAs to the E_1 one (2.91 eV) [25] of GaAs cannot be excluded due to the small difference between the two energy values. At low energy, the band gap of GaAs is clearly distinguishable in the ε spectra at about 1.4 eV. Also, the second energy derivative spectrum (Fig. 5) shows an interband transition at 1.75 eV which corresponds to the $E_0+\Delta_0$ CP energy of GaAs [25]. It is known that ε_2 is a gauge of material quality, the highest value implies the most abrupt interface [27]. Compared to literature values (~25), the highest values of ε_2 (26.8) in our case, obtained in the region of the E_2 band gap near 4.7 eV,

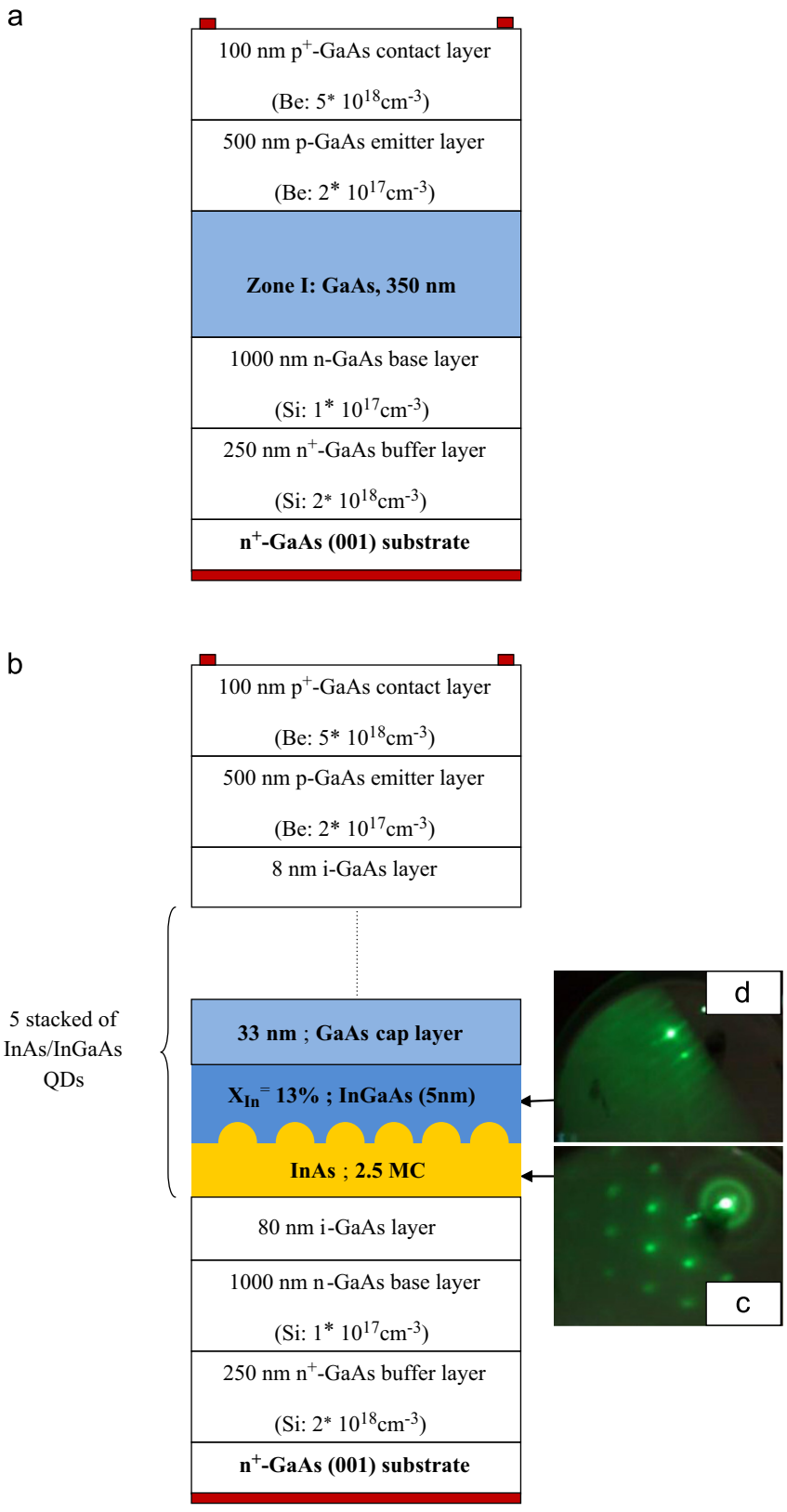

Fig. 1. Schematic layer structure of the GaAs reference SC (a) and a multi-layer stacked InAs/InGaAs QDs SC (b) grown on (001) n^+-GaAs substrate. RHEED patterned after growth of 2.5 ML of InAs (three dimensional growth) (c). RHEED patterned during growth of 5 nm InGaAs (two dimensional growth) (d).

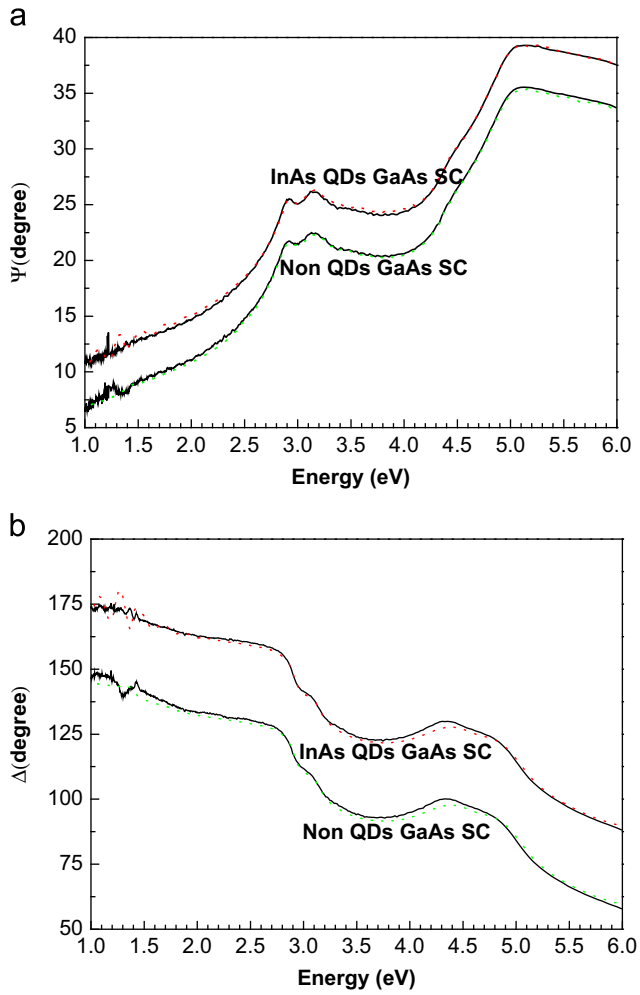

Fig. 2. Room temperature SE spectra of ψ (a) and Δ (b) for the two devices. The two spectra are vertically shifted for clarity. Also shown is a best fit (dots) using the model structure of Fig. 1.

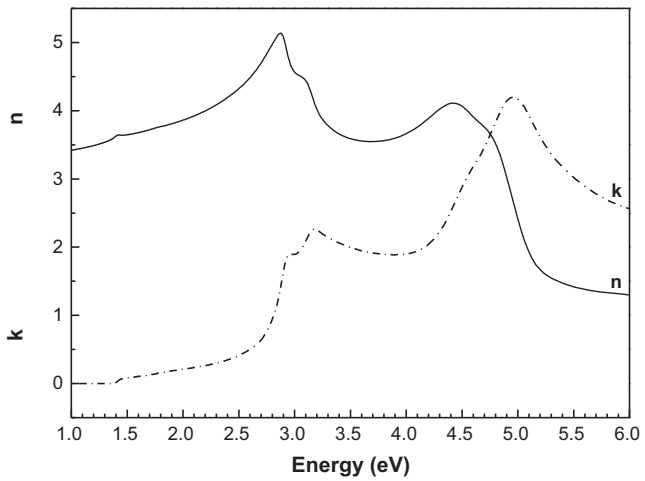

Fig. 3. The measured effective refraction index n and the extinction coefficient k of the InAs QDs SC.

indicate the high quality of materials forming the GaAs-based SCs grown by SS-MBE.

Fig. 6 shows the PL spectrum for the QDs SC under a low excitation power density of 25 mW at low-temperature. Obviously, this spectrum presents an asymmetric shape located in the

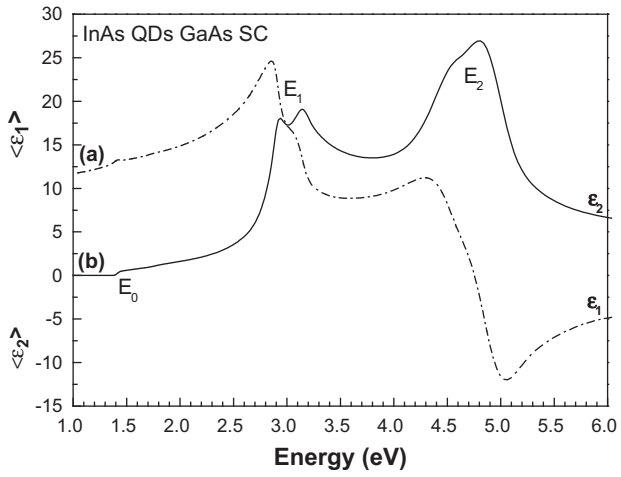

Fig. 4. Real (ε_1) and imaginary (ε_2) parts of dielectric functions of the InAs/InGaAs QDs SC obtained from SE measurements.

Table 1
Comparison between the different CP energies of GaAs and InAs obtained in our work and those of Refs. 25 and 26.

CP Energy	E_0(eV)	$E_0+\Delta_0$(eV)	E_1(eV)	$E_1+\Delta_1$(eV)	E_0'(eV)	E_2(eV)
Our data	1.4	1.75	2.88	3.09	4.39	4.73
GaAs: Ref. 25	1.42	1.75	2.91	3.14	4.45	4.77
InAs: Ref. 26	–	–	2.48	2.74	4.39	4.71

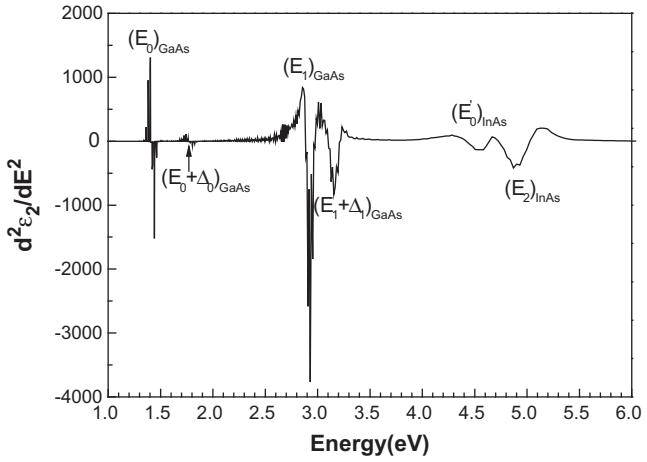

Fig. 5. Second-derivative spectrum of imaginary part (ε_2) of dielectric function as function of the photon energy for the InAs/InGaAs QDs SC. The transition energies arising from InAs QD layers and GaAs layers are indicated.

high-energy side and which can be deconvoluted in two sub-bands by Gaussian fitting [28]. As a result of Gaussian fitting dependent PL measurements, the two peaks are located at 1.06 eV and 1.11 eV. Considering the size distribution and areal densities of both QDs families, the most intense peak at 1.06 eV is attributed to larger (L) QDs, while the higher energy and larger peak at 1.11 eV refers to the larger number of relatively smaller (rS) QDs. In addition, peaks originating from both InGaAs quantum well layer and GaAs substrate are seen at around 1.35 eV, and 1.50 eV, respectively.

Fig. 7 shows the spectral response (SR) and the PL spectra at room temperature for the two GaAs-based SCs. As seen in Fig. 7(a), the photocurrent signal for the GaAs reference SC rapidly fall off at the GaAs band edge near 880 nm (1.42 eV) (photons with energy below the band gap produce no photocurrent in the

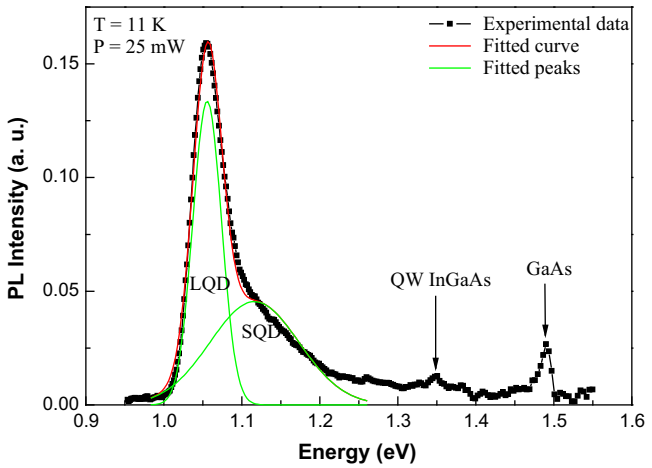

Fig. 6. PL spectrum measured at low temperature (11 K) from the 5 stacked layers of InAs/InGaAs QDs SC.

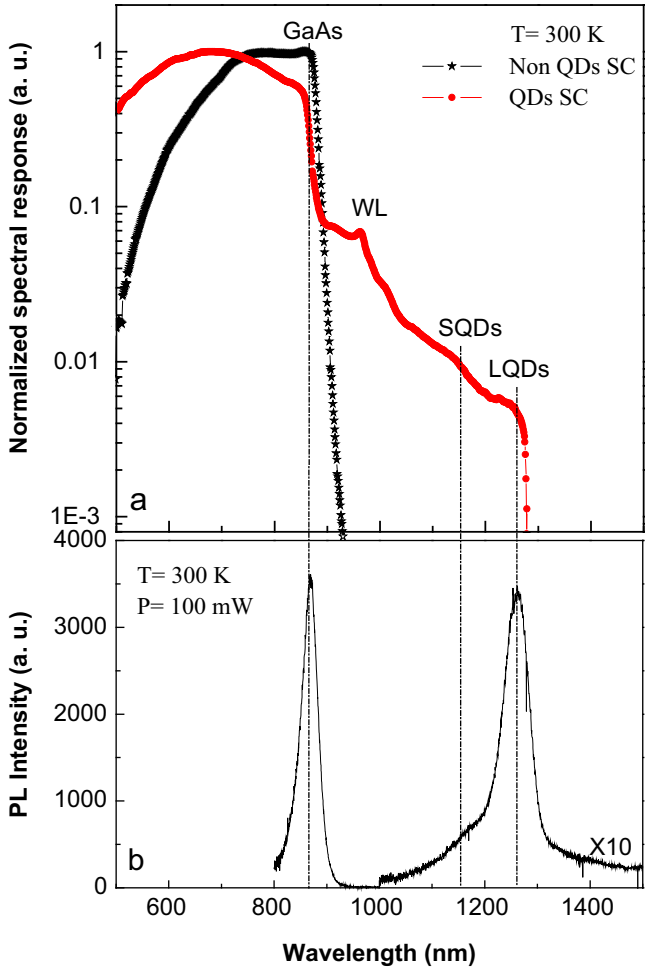

Fig. 7. Normalized spectral response for the two GaAs-based SCs with and without InAs QDs (a) and PL spectra of the two SCs at room temperature under an excitation power of 100 mW (b).

cell). However, the QDs SC shows an extended response up to 1280 nm (Fig. 7(a)) due to absorption from InAs QDs, wetting layer (WL) and InGaAs layer of the InAs/InGaAs QD heterostructure, i.e., intermediate band. Furthermore, the spectral response peak near $\lambda = 1000$ nm is induced by the WL [29,30] and the photo-generated current between 880–1000 nm (1.24–1.42 eV) is due to the absorption from InGaAs layer [31], while that beyond 1000 nm (< 1.24 eV) is due to InAs QDs absorption [18,32]. Broadening the range of absorption of the QDs SC spectrum is due to using a mixture of QDs of different sizes (LQD and rSQD) for harvesting the maximum proportion of the incident light and achieved the highest possible solar-electric conversion. The room temperature PL spectra (Fig. 7(b)) show a GaAs emission near 900 nm, a ground state emission from the rSQDs near 1150 nm and a ground state from the LQDs near a 1300 nm of the QDs SC. The optical transitions are consistent with the PL and SR spectra.

Finally, the SR for the 5 stacks InAs/InGaAs/GaAs QDs heterostructure SC is larger than those for InAs/GaAsN [33] and InGaAs [34] QD SCs grown, respectively, with and no strain compensation techniques. These results indicate that the multistacked InAs/InGaAs/GaAs QDs heterostructure SC has better cell characteristics. However, further effort is needed to increase the absorption in the infrared region by optical management and QD/barrier material combinations that have an electronic structure and absorption properties more suitable for QDs SC systems.

4. Conclusion

In conclusion, we have successfully fabricated GaAs-based SC with a multistack of InAs QDs by capping an InGaAs layer on the QDs and inserting GaAs spacer layers. The two major spectral features observed in the dielectric function spectra of the InAs QDs SC at ~3 eV and ~4.5 eV are attributed to the E_1 and E_2 CP structures of GaAs and InAs, respectively. The PL spectrum of the InAs QDs in the GaAs matrix is higher and presents an asymmetric shape, which indicated the growth of a high-quality multistacked InAs QDs structure and the contribution of larger and relatively smaller QDs to PL. The photocurrent measurement of InAs QDs SC demonstrates an extended photoresponse up to 1280 nm due to the absorption of low-energy photon by the QDs, which indicates that the InAs QDs SC has good cell characteristics. The InAs QDs facilitate the fabrication of highly stacked QD layers, which are suitable for SC devices that require QD layers for sufficient light absorption and performance improvement.

References

[1] D.E. Hasti, D.L. King, J.D. McBrayer, Crystalline photovoltaic research, status, and future direction, IEEE Photovoltaic Specialists Conferance (1990) 217–221.
[2] T. Ohshima, S. Sato, M. Imaizumi, T. Nakamura, T. Sugaya, K. Matsubara, S. Niki, Change in the electrical performance of GaAs solar cells with InGaAs quantum dot layers by electron irradiation, Solar Energy Materials and Solar Cells 108 (2013) 263–268.
[3] T. Sugaya, A. Takeda, R. Oshima, K. Matsubara, S. Niki, Y. Okano, InGaP-based InGaAs quantum dot solar cells with GaAs spacer layer fabricated using solid-source molecular beam epitaxy, Applied Physics Letters 101 (2012) 133110–133113.
[4] M.A. Green, A.W. Blakers, J. Zhao, A.M. Milne, A. Wang, X. Dai, Characterization of 23-percent efficient silicon solar cells, IEEE Transactions on Electron Devices 37 (1990) 331–335.
[5] M.R. Melloch, S.P. Tobin, C. Bajgar, T.B. Stellwag, A. Keshavarzi, M.S. Lundstorm, K. Emery, High-efficiency GaAs and AlGaAs solar cells grown by molecular beam epitaxy, IEEE Photovoltaic Specialists Conferance (1990) 163–167.
[6] A. Luque, S. Hegedus, Handbook of Photovoltaic Science and Engineering, John Wiley & Sons, Chichester, England, 2003.
[7] S.J. Taylor, A. Leycuras, B. Beaumont, C. Coutal, J.C. Roustan, A. Azema, in: Proceedings of the 22nd IEEE Photovoltaic Specialist Conference, Waikolaa, Hawaii, 1994.
[8] C.O. Mc Pheeters, C.J. Hill, S.H. Lim, D. Derkacs, D.Z. Ting, E.T. Yu, Improved performance of In(Ga)As quantum dot solar cells via light scattering by nanoparticles, Journal of Applied Physics 106 (2009) 056101–056103.
[9] C. Jiang Wua, V.R. Manghama, M.O. Reddy, B.D. Manasreh, Weaver, surface plasmon enhanced intermediate band based quantum dots solar cell, Solar Energy Materials and Solar Cells 102 (2012) 44–49.

[10] R. Oshima, Y. Okada, A. Takata, S. Yagi, K. Akahane, R. Tamaki, K. Miyano, High-density quantum dot superlattice for application to high-efficiency solar cells, Physica Status Solidi C 8 (2011) 619–621.
[11] X.J. Shang, J.F. He, M.F. Li, F. Zhan, H.Q. Ni, Z.C. Niu, H. Pettersson, Y. Fu, Quantum-dot-induced optical transition enhancement in InAs quantum-dot-embedded p-i-n GaAs solar cells, Applied Physics Letters 99 (2011) 113514–113517.
[12] A. Marti, L. Cuadra, A. Luque, Design constraints of the quantum-dot intermediate band solar cell, Physica E 14 (2002) 150–157.
[13] T. Trupke, M.A. Green, P. Würfel, Improving solar celle fficiencies by up-conversion of sub-band-gap light, Journal of Applied Physics 92 (2002) 4117–4122.
[14] C.Y. Ngo, S.F. Yoon, W.J. Fan, S.J. Chua, Effects of size and shape on electronic states of quantum dots, Physical Review B 74 (2006) 245331–24540.
[15] A. Martí, N. López, E. Antolín, E. Cánovas, A. Luque, C.R. Stanley, C.D. Farmer, P. Díaz, Emitter degradation in quantum dot intermediate band solar cells, Applied Physics Letters 90 (2007) 233510–233512.
[16] C.Y. Ngo, S.F. Yoon, W.J. Fan, S.J. Chua, Tuning InAs quantum dots for high areal density and wideband emission, Applied Physics Letters 90 (2007) 113103–113105.
[17] C.Y. Ngo, S.F. Yoon, C.Z. Tong, W.K. Loke, S.J. Chua, An investigation of growth temperature on the surface morphology and optical properties of 1.3 μm InAs/InGaAs/GaAs quantum dot structures, Nanotechnology 18 (2007) 365708–365708.
[18] L. Marti, N. Lopez, E. Antolin, E. Canovas, A. Luque, C. Stanley, C. Farmer, P. Diaz, Emitter degradation in quantum dot intermediate band solar cells, Applied Physics Letters 90 (2007) 233510–233513.
[19] R. Oshima, A. Takata, Y. Okada, Strain-compensated InAs/GaNAs quantum dots for use in high-efficiency solar cells, Applied Physics Letters 93 (2008) 083111–083111.
[20] J.M. Moison, C. Guille, F. Houzay, F. Barthe, M. Van Rompay, Surface segregation of third-column atoms in group III–V arsenide compounds, ternary alloys and heterostructures, Physical Review B 40 (1989) 6149–6162.
[21] R.M.A. Azzam, N.M. Bashara, Ellipsometry and Polarized Light, Elsevier Science, New York, 1989.
[22] D.E. Aspnes, Handbook of Optical Constants of Solids, in: E.D. Palik (Ed.), Academic, 1991.
[23] S.Y. Lee, J.H. Shim, D.J. You, S. Ahn, H.M. Lee, The novel usage of spectroscopic ellipsometry for the development of amorphous Si solar cells, Solar Energy Materials and Solar Cells 95 (2011) 142–145.
[24] C. Major, G. Juhász, P. Petrik, Z. Horváth, O. Polgár, M. Fried, Application of wide angle beam spectroscopic ellipsometry for quality control in solar cell production, Vacuum 84 (2010) 119–122.
[25] S. Ozaki, S. Adachi, Spectroscopic ellipsometry and thermoreflectance of GaAs, Journal of Applied Physics 78 (1995) 3380–3386.
[26] T.J. Kim, J.J. Yoon, S.Y. Hwang, Y.W. Jung, T.H. Ghong, Y.D. Kim, H. Kim, Y.C. Chang, InAs critical-point energies at 22 K from spectroscopic ellipsometry, Applied Physics Letters 97 (2010) 171912–171914.
[27] D.E. Aspnes, A.A. Studna, Chemical etching and cleaning procedures for Si, Ge, and some III–V compound semiconductors, Applied Physics Letters 39 (1981) 316–318.
[28] J. Rihani, V. Sallet, N. Yahyaoui, J.C. Harmand, M. Oueslati, R. Chtourou, Interdot carrier's transfer via tunneling pathway studied from photoluminescence spectroscopy, Journal of Luminescence 129 (2009) 251–255.
[29] K.Y. Chuang, E.T. Tzeng, Y.C. Liu, K.D. Tzeng, T.S. Lay, Photovoltaic response of coupled InGaAs quantum dots, Journal of Crystal Growth 323 (2011) 508–510.
[30] E.S. Shatalina, S.A. Blokhin, A.M. Nadtochy, A.S. Payusov, A.V. Savelyev, M.V. Maximov, A.E. Zhukov, N.N. Ledentsov, A.R. Kovsh, S.S. Mikhrin, V.M. Ustinov, Analysis of mechanisms of carriers emission in the p-i-n structures with In(Ga)As quantum dots, Semiconductors 44 (2010) 1308–1312.
[31] C.Y. Ngo, S.F. Yoon, W.K. Loke, T.K. Ng, Photovoltaic characteristics of InAs/InGaAs/GaAs QD heterostructures, Journal of Crystal Growth 311 (2009) 1885–1888.
[32] Y. Okada, R. Oshima, A. Takata, Characteristics of InAs/GaNAs strain-compensated quantum dot solar cell, Applied Physics Letters 106 (2009) 24306–24309.
[33] R. Oshima, A. Takata, Y. Shoji, K. Akahane, Y. Okada, InAs/GaNAs strain-compensated quantum dots stacked up to 50 layers for use in high-efficiency solar cell, Physica E 42 (2010) 2757–2760.
[34] T. Sugaya, Y. Kamikawa, S. Furue, T. Amano, M. Mori, S. Nik, Multi-stacked quantum dot solar cells fabricated by intermittent deposition of InGaAs, Solar Energy Materials and Solar Cells 95 (2011) 163–166.